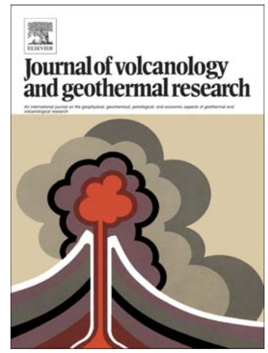

Uncertainties in volcanic plume modeling: A parametric study using FPLUME

G. Macedonio, A. Costa, A. Folch

PII: S0377-0273(16)30028-2
DOI: doi: 10.1016/j.jvolgeores.2016.03.016
Reference: VOLGEO 5797

To appear in: *Journal of Volcanology and Geothermal Research*

Received date: 30 November 2015
Revised date: 15 March 2016
Accepted date: 22 March 2016

Please cite this article as: Macedonio, G., Costa, A., Folch, A., Uncertainties in volcanic plume modeling: A parametric study using FPLUME, *Journal of Volcanology and Geothermal Research* (2016), doi: 10.1016/j.jvolgeores.2016.03.016

Uncertainties in volcanic plume modeling: a parametric study using FPLUME

G. Macedonio[a,*], A. Costa[b], A. Folch[c]

[a]Istituto Nazionale di Geofisica e Vulcanologia, Osservatorio Vesuviano, Napoli, Italy
[b]Istituto Nazionale di Geofisica e Vulcanologia, Bologna, Italy
[c]Barcelona Supercomputing Center, Barcelona, Spain

Abstract

We carry out a parametric study in order to identify and quantify the effects of uncertainties on pivotal parameters controlling the dynamics of volcanic plumes. The study builds upon numerical simulations using FPLUME, an integral steady-state model based on the Buoyant Plume Theory generalized in order to account for volcanic processes (particle fallout and re-entrainment, water phase changes, effects of wind, etc). As reference cases for strong and weak plumes, we consider the cases defined during the IAVCEI Commission on tephra hazard modeling inter-comparison study (Costa et al., 2016). The parametric study quantifies the effect of typical uncertainties on total mass eruption rate, column height, mixture exit velocity, temperature and water content, and particle size. Moreover, a sensitivity study investigates the role of wind entrainment and intensity, atmospheric humidity, water phase changes, and particle fallout and re-entrainment. Results show that the leading-order parameters that control plume height are the mass eruption rate and the air entrainment coefficient, especially for weak plumes.

Keywords: Volcanic plumes, Buoyant Plume Theory, FPLUME, Uncertainty

1. Introduction

Tephra Transport and Dispersal Models (TTDMs; Folch, 2012) are commonly used for volcanic hazard assessment and tephra dispersal (ash cloud) forecasts. The proper quantification of the parameters defining the source term in TTDMs, and in particular the estimation of the Mass Eruption Rate (MER), plume height, and particle vertical mass distribution, is of paramount importance for obtaining reliable results in terms of particle mass concentration in the atmosphere and loading on the ground. Several TTDMs (*e.g.* FALL3D; Costa et al. (2006); Folch et al. (2009); ASH3D; Schwaiger et al. (2012)) can

*Corresponding author
Email addresses: giovanni.macedonio@ingv.it (G. Macedonio), antonio.costa@ingv.it (A. Costa), arnau.folch@bsc.es (A. Folch)

obtain the source term through coupling with 1D integral plume models, which describe the plume dynamics depending on vent and atmospheric conditions. As a result, uncertainties in plume modeling (*e.g.* in vent conditions, state of the atmosphere, or implicit in the plume model parameterizations) result in uncertain Eruption Source Parameters (ESPs) and propagate to TTDMs strongly affecting its accuracy.

We perform a parametric and a sensitivity study to quantify how typical uncertainties in vent conditions and plume model parameterizations affect the ESPs, and in particular the plume height. To this purpose, we use FPLUME (Folch et al., 2016), a steady-state 1-D cross-section averaged eruption column (plume) model based on the Buoyant Plume Theory (BPT) firstly developed by Morton et al. (1956) and later adapted for volcanic plumes (e.g. Woods, 1988, 1993; Ernst et al., 1996; Bursik, 2001). FPLUME accounts for plume bent over by wind, entrainment of ambient moisture, effects of water phase changes, particle fallout and re-entrainment, a parameterization for the wind entrainment coefficients based on the local Richardson number and a model for wet aggregation of ash particles in the presence of liquid water or ice. Our study focuses on the two reference cases (strong and weak plumes) defined during the volcanic plume model inter-comparison study promoted by the IAVCEI Commission of tephra hazard modeling (Costa et al., 2016). Because of the large number of parameters that can affect plume dynamics, our studies fix the particle grain size distributions and wind profiles for both strong and weak plume.

2. Physical Model

This section summarizes the governing equations and parameterization of the FPLUME model (for a more detailed description see Folch et al., 2016). FPLUME is a 1D steady-state volcanic plume model based on the Buoyant Plume Theory of Morton et al. (1956) that accounts for different options for estimating air entrainment (Carazzo et al., 2006, 2008b; Tate & Middleton, 2000), plume bending due to wind effects (Bursik, 2001), fallout of particles from the plume (Bursik, 2001), particle re-entrainment (Ernst et al., 1996), water phase changes (Woods, 1988, 1993), particle wet aggregation (Costa et al., 2010; Brown et al., 2012), and column collapse. The model considers the volcanic plume as a multiphase mixture of volatiles, suspended particles (tephra), and entrained ambient air. For simplicity, water (in vapor, liquid or ice phase) is assumed to be the only volatile species, being either of magmatic or phreatic origin, or incorporated trough the ingestion of moist ambient air. Since the governing equations based upon the BPT are not adequate above Neutral Buoyancy Level (NBL), the model uses a semi-empirical approach above this region (see Folch et al. (2016)).

2.1. Governing Equations

The equations solved by FPLUME up to the NBL are obtained assuming steady-state cross-section averaged equations for axisymmetric plume motion in a turbulent wind (Folch et al., 2016):

$$\frac{d\hat{M}}{ds} = 2\pi r \rho_a u_e + \sum_{i=1}^{n} \frac{d\hat{M}_i}{ds} \tag{1a}$$

$$\frac{d\hat{P}}{ds} = \pi r^2 \left(\rho_a - \hat{\rho}\right) g \sin\theta + u_a \cos\theta \left(2\pi r \rho_a u_e\right) + \hat{u} \sum_{i=1}^{n} \frac{d\hat{M}_i}{ds} \tag{1b}$$

$$\hat{P} \frac{d\theta}{ds} = \pi r^2 \left(\rho_a - \hat{\rho}\right) g \cos\theta - u_a \sin\theta \left(2\pi r \rho_a u_e\right) \tag{1c}$$

$$\frac{d\hat{E}}{ds} = 2\pi r \rho_a u_e \left((1 - w_a) c_a T_a + w_a h_{wa}(T_a) + gz + \frac{1}{2} u_e^2 \right) + c_p \hat{T} \sum_{i=1}^{n} \frac{d\hat{M}_i}{ds} \tag{1d}$$

$$\frac{d\hat{M}_a}{ds} = 2\pi r \rho_a u_e (1 - w_a) \tag{1e}$$

$$\frac{d\hat{M}_w}{ds} = 2\pi r \rho_a u_e w_a \tag{1f}$$

$$\frac{d\hat{M}_i}{ds} = -\frac{\chi u_{si}}{r \hat{u}} \left(1 + \frac{f u_e}{u_{si} dr/ds}\right)^{-1} \hat{M}_i + A_i^{+} - A_i^{-} \tag{1g}$$

$$\frac{dx}{ds} = \cos\theta \cos\Phi_a \tag{1h}$$

$$\frac{dy}{ds} = \cos\theta \sin\Phi_a \tag{1i}$$

$$\frac{dz}{ds} = \sin\theta \tag{1j}$$

where $\hat{M} = \pi r^2 \hat{\rho} \hat{u}$ is the total mass flow rate, $\hat{P} = \hat{M} \hat{u}$ is the total axial (stream-wise) momentum flow rate, θ is the plume bent over angle with respect to the horizontal (*i.e.* $\theta = 90°$ for a plume raising vertically), $\hat{E} = \hat{H} + \hat{M}(gz + \frac{1}{2}\hat{u}^2)$ is the total energy flow rate, $\hat{H}$ is the enthalpy flow rate of the mixture, $\hat{T} = \hat{T}(\hat{H})$ is the mixture temperature, $\hat{M}_a$ is the mass flow rate of dry air, $\hat{M}_w = \hat{M} x_w$ is the mass flow rate of water, x_w is the mass fraction of water (including water vapor, liquid and ice, *i.e.* $x_w = x_v + x_l + x_s$), $\hat{M}_i = \hat{M} x_p f_i$ is the mass flow rate of particles of class i ($i = 1 : n$ where n is the number of particle classes), x and y are the horizontal coordinates, z is height, s is the distance along the plume axis and Φ_a is the horizontal wind direction (azimuth). The complete list of symbols and variables is reported in Tables 1 and 2. The equations above express the conservation of total mass (1a), stream-wise (1b) and radial (1c) momentum, energy (1d), mass of dry air (1e), mass of water (1f), and mass of particles (1g). Finally, eqs. (1h) to (1j) determine the 3D plume trajectory as a function of the length parameter s. The hat above a variable denotes "bulk" quantities, that is, a variable integrated over a plume cross-section using a top-hat profile in which a generic quantity ϕ has a constant value $\hat{\phi}(s)$ at a given plume cross-section and vanishes outside. These equations constitute a set of

$9+n$ first order ordinary differential equations in s for $9+n$ unknowns: $\hat{M}$, $\hat{P}$, θ, $\hat{E}$, $\hat{M}_a$, $\hat{M}_w$, $\hat{M}_i$ (for each particle class), x, y and z. Please, note that the last term in eq. (1b) represents the change in stream-wise momentum due to loss or re-entrainment of the particles. However, while particles leave the column with velocity $\hat{u}$, re-entrained particles enter with the velocity of the environment air. For simplicity, the difference between outgoing and ingoing particle velocity is not taken into account and we assume that re-entrained particles enter the plume with velocity $\hat{u}$. However, such an assumption introduces in the momentum balance equation a negligible error (less than a few percent in the investigated cases).

The enthalpy flow rate of the mixture is a non-decreasing function of the temperature $\hat{T}$, given by:

$$\hat{H} = \hat{M}[x_a c_a \hat{T} + x_p c_p \hat{T} + x_v h_v(\hat{T}) + x_l h_l(\hat{T}) + x_s h_s(\hat{T})] \tag{2}$$

where h_v, h_l and h_s are, respectively, the enthalpy per unit mass of water vapor, liquid and ice:

$$h_s(\hat{T}) = c_s \hat{T} \tag{3a}$$

$$h_l(\hat{T}) = h_{l0} + c_l(\hat{T} - T_0) \tag{3b}$$

$$h_v(\hat{T}) = h_{v0} + c_v(\hat{T} - T_0) \tag{3c}$$

where $c_s = 2108\,\mathrm{J\,K^{-1}kg^{-1}}$ is the specific heat of ice, T_0 is a reference temperature, $h_{l0} = 3.337\times10^5\,\mathrm{J\,kg^{-1}}$ is the enthalpy of the liquid water at the reference temperature, $c_l = 4187\,\mathrm{J\,K^{-1}kg^{-1}}$ is the specific heat of liquid water, $h_{v0} = 2.501\times10^6\,\mathrm{J\,kg^{-1}}$ is the enthalpy of vapor water at the reference temperature and $c_v = 1996\,\mathrm{J\,K^{-1}kg^{-1}}$ is the specific heat of vapor water. For convenience, the reference temperature T_0 is taken equal to the temperature of triple point of the water ($T_0 = 273.15\,\mathrm{K}$). The energy and the enthalpy flow rate are related by:

$$\hat{E} = \hat{H} + \hat{M}(gz + \frac{1}{2}\hat{u}^2) \tag{4}$$

For the integration of eq. (1d) and for evaluating the aggregation rate terms in eq. (1g), the temperature $\hat{T}$ and the mass fractions of ice (x_s), liquid water (x_l) and vapour (x_v) need to be evaluated. These quantities are obtained by the direct inversion of eq. (2), with the use of eqs. (1d) and (4) and by assuming that the pressure inside the plume P is equal to the atmospheric pressure at the same altitude (z).

The model uses a pseudo-gas assumption considering that the mixture of air and water vapour behaves as an ideal gas:

$$P = P_v + P_a\ ; \qquad P_v = n_v P\ ; \qquad P_a = n_a P \tag{5a}$$

$$n_v = \frac{x_v/m_v}{x_v/m_v + x_a/m_a}\ ; \qquad n_a = \frac{x_a/m_a}{x_v/m_v + x_a/m_a} \tag{5b}$$

where P_v and P_a are, respectively the partial pressures of the water vapour and of the air in the plume, n_v and n_a are the molar fractions of vapour and air in the gas phase ($n_v + n_a = 1$) and $m_v = 0.018\,\mathrm{kg/mole}$ and $m_a = 0.029\,\mathrm{kg/mole}$ are the molar weights of vapour and air.

For the particle re-entrainment parameter f in eq. (1g) we adopt the fit proposed by Bursik (2001) on the basis of the experimental results of Ernst et al. (1996) for plumes not affected by wind:

$$f = 0.43\left(1 + \left[\frac{0.78 u_s P_o^{1/4}}{F_o^{1/2}}\right]^6\right)^{-1} \tag{6}$$

where $P_o = r_o^2 \hat{u}_o^2$ and $F_o = r_o^2 \hat{u}_o \hat{c}_o \hat{T}_o$ are the specific momentum and thermal fluxes at the vent ($s = 0$) (see Folch et al., 2016, for more details).

Particle terminal settling velocity u_{si} is parameterized as Costa et al. (2006); Folch et al. (2009):

$$u_{si} = \sqrt{\frac{4g(\rho_{pi} - \hat{\rho})d_i}{3C_d\hat{\rho}}} \tag{7}$$

where d_i is the class particle diameter and C_d is a drag coefficient that depends on the Reynolds number $Re = d_i u_{si} \hat{\rho}/\hat{\mu}$. Here we use the parameterisation proposed by Ganser (1993), which considers the effects of particles sphericity Ψ.

2.2. Solving Strategies

Given a closure equation for the turbulent air entrainment velocity (u_e) and an aggregation model (defining the mass aggregation coefficients A_i^+ and A_i^-), eqs. (1a) to (1j) can be integrated along the plume axis from the inlet (volcanic vent) up to the NBL. Inflow (boundary) conditions are required at the vent ($s = 0$) for total MER $\hat{M}_o$ (*i.e.* the total mass flow rate at the vent), bent over angle $\theta_o = 90°$, temperature $\hat{T}_o$, exit velocity $\hat{u}_o$, fraction of water x_{wo}, null air mass flow rate $\hat{M}_a = 0$, vent coordinates (x_o,y_o and z_o), and MER for each particle class $\hat{M}_{io}$. The latter is obtained from the total MER given the particle grain size distribution at the vent:

$$\hat{M}_{io} = f_{io}\hat{M}_o(1 - x_{wo}) \tag{8}$$

where f_{io} is the mass fraction of class i at the vent.

Alternatively, equations can also be solved given the plume height rather than the total MER at the vent $\hat{M}_o$. The inverse problem of finding $\hat{M}_o$ from an assigned height is solved by changing $\hat{M}_o$ iteratively until the obtained column height approximates the required value within a specified tolerance ($\approx$10 m). The search algorithm is based on the bisection method. However, although the direct method (find height h given $\hat{M}_o$) always gives a solution, the inverse problem cannot always find a $\hat{M}_o$ that gives a required column height. The reason for this is the non-linear relationship between MER and column height due to air stratification, wind, column collapse conditions, etc.

3. Parametric study on the input parameters

Firstly, we performed a parametric study of the model inputs to quantify how uncertainties at the vent (*i.e* on $\hat{M}_o$, $\hat{u}_o$, $\hat{T}_o$, x_{wo}, and particle size) affect the Eruption Source Parameters (ESP). Emphasis is given on plume height because of its pivotal role on atmospheric dispersal. Our study focus on the two test cases defined in the IAVCEI inter-comparison study (Costa et al., 2016) for strong and weak plumes considering both windy and windless conditions. For the strong plume scenario, meteorological data were obtained from the European Centre for Medium-Range Weather Forecasts (ECMWF) and corrected above 20 km by Costa et al. (2013) for Pinatubo volcano at 13:40 PLT of 15 June 1991 (column height 39 km). For the weak plume scenario, meteorological data were provided by the Japan Meteorological Agency's Non-Hydrostatic Model (Hashimoto et al., 2012) for Shinmoe-dake volcano at 00:00 JST on 27 January 2011 (column height 8 km).

The parametric study consists on a series of runs varying the model input parameters one at a time. When possible, the rest of the parameters are kept constant as in the reference case (see Table 3) or are modified for ensuring a physical consistency. In particular, at the vent, the mass eruption rate $\hat{M}_o$, the density of the mixture $\hat{\rho}_o = \hat{\rho}_0(P_0, \hat{T}_0, x_{w0})$, the exit velocity $\hat{u}_0 = \hat{u}_0(P_0, \hat{T}_0, x_{w0})$ and the vent radius r_0 are related by the relationship:

$$\hat{M}_0 = \pi r_0^2 \hat{\rho}_0 \hat{u}_0 \tag{9}$$

where P_0 is the pressure at the vent, assumed equal to the atmospheric pressure at the same quote. In this study, unless otherwise specified, when a single parameter among $\hat{M}_0$, $\hat{T}_0$, $\hat{x}_{w0}$, $\hat{u}_0$ is varied, then the vent radius r_0 is modified accordingly, in order to satisfy eq. (9). For the reference case, according to the values of Table 3), vent radius and column density at the vent are, respectively, 708 m and 3.46 kg/m^3 for the strong plumes, and 27 m and 4.85 kg/m^3 for the weak plumes.

The response of the model was explored within the following ranges, representative of typical uncertainties at the vent:

1. Total MER $\hat{M}_o$ ranging from 1/5 to 5 times the reference values (1.5×10^9 and 1.5×10^6 kg/s for strong and weak plumes, respectively);
2. Eruption column heights varying ±20% with respect the reference values;
3. Mixture exit velocities $\hat{u}_o$ varying ±30% with respect the reference values (275 and 135 m/s for strong and weak);
4. Mixture exit temperatures $\hat{T}_o$ varying ±100 K with respect the reference values (1053 and 1273 K for strong and weak);
5. Erupted water mass fraction x_{wo} varying ±2 wt% with respect the reference values (5 and 3% for strong and weak).

The grain size distributions for both strong and weak plumes were assumed as in Costa et al. (2016) and are reported in Table 4. However, in order to explore the role of particle size we also considered additional runs with a single particle class varying $\pm 6\Phi$ with respect a reference value of $\Phi = 2$ (250 μm).

3.1. Effect of MER variations on height

Figure 1 shows the variation of the column height h as function of the total MER at the vent $\hat{M}_o$. The mass flow rate is changed by varying the vent radius, keeping constant the exit velocity, the temperature and the water mass fraction at the vent (see Table 3). In the investigated range of MER, the vent radius varies from 317 to 1583 m for the strong plumes and from 12 to 61 m for the weak plumes. Results are given as absolute and relative variations, the latter showing the column height variation factor h/h^{ref} given a relative MER variation $100 \times (\hat{M}_o - \hat{M}_o^{\mathrm{ref}})/\hat{M}_o^{\mathrm{ref}}$ ranging from -80 to 400. This range corresponds to a variation between 1/5 and 5 of the ratio $\hat{M}_o/\hat{M}_o^{\mathrm{ref}}$. As expected (see eg. Wilson et al., 1978; Bursik & Woods, 1991; Bursik, 2001; Degruyter & Bonadonna, 2012), the column height increases with $\hat{M}_o$ following approximately a power law. Note how, for windless conditions, the strong plume collapses at MERs larger than about 4.9×10^9 kg/s whereas, in the presence of wind, the collapse is not observed because the increased entrainment of air. This result is consistent with the work of Degruyter & Bonadonna (2013) who find that wind increases air entrainment and prevents column collapse.

3.2. Effect of vent radius variations on height

The effect of the variation of the vent radius on the column height is implicitly contained in the results obtained by varying the MER. In fact, according to eq. (9), keeping constant $\hat{T}_0$ (i.e. ρ_0, under the assumption that the exit pressure equals the atmospheric pressure) and $\hat{u}_0$, a variation of $\hat{M}_0$ is equivalent to a variation of r_0. Referring to Figure 1, for the strong plumes, the vent radius varies from 317 m for MER 3×10^8 kg/s to 1583 m for MER 7.5×10^9 kg/s. For strong plumes, in the windless condition, column collapse occurs for MER 4.9×10^9 kg/s, corresponding to a vent radius of 1293 m, For the weak plumes, the vent radius varies from 12 m for MER 3×10^5 kg/s to 61 m for MER 7.5×10^6 kg/s.

3.3. Effect of height variations on MER

In practice, it is more convenient to quantify the variations on $\hat{M}_o$ resulting from column height uncertainties because column height is much easier to observe (or, at least, to constrain). Results are shown in Figure 2 for relative variations $100 \times (h - h^{\mathrm{ref}})/h^{\mathrm{ref}}$ in the range $\pm20\%$ with respect the reference value h^{ref}. As observed, to produce an increase of only 10% in the column height requires of an increase in the MER by 50 and 25% for strong and weak plumes respectively. In other words, small errors (uncertainties) in column height measurements will result on much larger (relative) errors in the estimation of MER and, consequently, in the concentration downstream.

For the strong plumes, in the investigated range of column height (or mass eruption rate), Figures 1 and 2 show the presence of small bumps. These are related to the release of heat in the plume, due to the water phase change. The effect disappears when the latent heat for condensation of freezing of water are set equal to zero.

3.4. Effect of exit velocity variations on height

The effect of a variation in the mixture exit velocity $\hat{u}_o$ on column height is reported in Figure 3. The variation of the velocity is performed at constant MER, by adjusting the vent radius accordingly. In the investigated range of exit velocity, the vent radius varies from 621 to 846 m for the strong plumes and from 24 to 32 m for the weak plumes. The temperature and the water mass fraction at the vent was kept constant (see Table 3). As observed, column heights are almost insensitive to variations on exit velocities within the explored uncertainty range (±30% relative variations). However, for the strong plume case in windless conditions, columns collapse for velocities lower than about 220 m/s. This reflects the existence of a minimum value of $\hat{u}_o$ (or of $\hat{M}_o$) to sustain the plume buoyantly.

Moreover, the exit velocity was varied in the same ranges shown in Figure 3, but keeping fixed vent radius, exit temperature and water fraction (same as the reference case); MER is changed accordingly, in order to satisfy eq. (9). Results are not reported, since they do not differ significantly from Figure 3. In this case, for the strong plumes, in the windless condition, column collapse occurs for an exit velocity of 207 m/s, corresponding to a MER of 1.13×10^9 kg/s.

The effect of exit velocity on column collapse was previously described by Sparks & Wilson (1976), Wilson (1976), Wilson et al. (1978) and Wilson et al. (1980) who found that the conditions leading to collapse involve large vent radii, low gas velocities, and low gas contents. Similar results were also obtained by Valentine & Wohletz (1989); Kaminski & Jaupart (2001); Degruyter & Bonadonna (2013) and Dellino et al. (2014). Our findings are consistent with these previous works.

3.5. Effect of exit temperature variations on height

Most of the height of a volcanic eruption column is dominated by buoyancy effects (Sparks, 1986) and, to a first approximation, the height of the plume is related to the thermal flux at the vent (Wilson et al., 1978; Settle, 1978; Sparks, 1986). In the parametric study we varied the exit temperature keeping fixed the external (atmospheric) pressure, the mass eruption rate (MER) and the exit velocity. This implies that the density of the mixture at the vent varies as a consequence of the variation of the density of the gas phase (vapor). We assume that the gas density follows the equation of state of the ideal gas. In the investigated range of exit temperature, the vent radius varies from 673 to 741 m for the strong plumes and from 26 to 28 m for the weak plumes, whereas the density of the mixture at the vent varies from 3.1 to 3.7 kg/m^3 for the strong plumes and from 4.5 and 5.2 kg/m^3 for the weak plumes.

Results are reported in Figure 4 which shows the variation of column height h on mixture exit temperature $\hat{T}_o$ for variations in the range ±100 K the reference value. The effect of $\hat{T}_o$ is noticeable for strong plumes (*e.g.* an increase of 5% in $\hat{T}_o$ results on an increase of about 2.5% in column height) but negligible for weak plumes (as reflected by the flat lines in Fig. 4c and 4d).

3.6. Effect of the erupted water content variations on height

Figure 5 shows the effect of the erupted water mass fraction x_{wo} on the column height for relative variations (uncertainties) in the range ± 2 wt% the reference value. The water content, affecting the mixture density, was varied keeping constant the MER and the exit velocity. The vent radius was adjusted accordingly. In the investigated range of initial water content, the vent radius varies from 548 to 838 m for the strong plumes and from 16 to 35 m for the weak plumes. Column height slightly increases as the erupted water content increases. This effect is clear for strong plumes (*e.g.* an increase of 2 wt% results on an increase of about 2.5% in column height) but, as occurs with the mixture exit temperature, it is almost negligible for weak plumes.

3.7. Effect of particle size variations on height

In order to investigate the effect of particle size variations on column height we performed additional runs with a single granulometric class ranging $\pm 6\Phi$ with respect to a reference value. The densities of each particle class were set as in Costa et al. (2016) and are reported in Table 4. As shown in Figure 6, the effect of particle size is visible only for windless conditions and particles in the millimetric range. This result is consistent with the works of Woods & Bursik (1991); de' Michieli Vitturi et al. (2015); Pouget et al. (2016), who found negligible variations of the column height with mean grain size in the range ($-6 \leq \Phi \leq 0$). In contrast, because of a different assumption on the grain size distribution (i.e. a power-law number distribution) and a larger particle size range, results of Girault et al. (2014, 2016) indicate that column height can be significantly affected by particle size distribution.

4. Sensitivity study on model parameterizations

A sensitivity study was also performed on the FPLUME model parameters related to wind entrainment, wind intensity, water phase change, air humidity (moisture), and particle fallout and re-entrainment. The effect of these processes was investigated by turning on and off the corresponding term in the model equations or by varying the parameters controlling the process (*e.g.* for studying the effect of air entrainment in the column).

4.1. Effect of entrainment coefficients on column height

The amount of entrained air in the column is described by the entraining velocity u_e, usually parameterized as a function of the rising velocity of the column and the wind velocity (eg. Hewett et al., 1971; Bursik, 2001; Suzuki & Koyaguchi, 2015; Woodhouse et al., 2015; Folch et al., 2016):

$$u_e = \alpha|\hat{u} - u_a \cos\theta| + \beta|u_a \sin\theta| \qquad (10)$$

where $\hat{u}$ and u_a are, respectively, the velocity of the plume along the centerline and the velocity of the wind. In the FPLUME model α and β can be set as constants or calculated at each point depending on the local Richardson number (Tate, 2002; Carazzo et al., 2006, 2008b,a; Folch et al., 2016). For the test cases, we adopted the formulation based on the local Richardson number (Folch et al., 2016), predicting entrainment coefficients varying from 0.07 to 0.17 for α and from 0.43 to 1.00 for β. However, for the sensitivity study these parameters were assumed as constants varying in the ranges $\alpha = 0.05 - 0.15$ and $\beta = 0.1 - 1.0$, as dictated by Costa et al. (2016).

Figures 7a and 7c show the sensitivity of column height to variations in α for strong and weak plumes without wind (note that, for the windless case, $u_a = 0$ and β plays no role). Note how variations in α within the considered range imply variations of up to $\pm 20\%$ and $\pm 30\%$ for weak and strong plumes respectively. This effect is largely magnified when considering the combined effect of α and β. In the case of a weak plume, with stronger wind, the column height can decrease up to a factor 2.5 with respect to the reference value if $\beta \geq 0.5$ (see Fig. 7d).

4.2. Effect of wind velocity on height

In order to investigate the influence of wind velocity on column height, the reference wind profiles (from Costa et al. (2016)) were multiplied by a factor f_w ranging between 0 and 2 (a value of $f_w = 1$ indicates the reference wind used in this work whereas a value of $f_w = 0$ corresponds to plumes in windless conditions). The resulting sensitivity of column height is shown in Figure 8. As expected, plume bending increases with wind, resulting on a decrease of plume height (see e.g. Bursik, 2001; Folch et al., 2012; Devenish, 2013; Woodhouse et al., 2013; Mastin, 2014). Because of the stronger intensity characterizing the reference wind profile, the effect is more pronounced for the weak plumes, with differences of up to 80% between windless and reference windy conditions.

4.3. Effects of various physical processes on height

In addition to the parameters described above, the height of the volcanic column is affected by various processes such as water phase change, entrainment of moisture, particle fallout and re-entrainment. The effect of the moisture and water phase change in the plume was previously investigated by Woods (1993) who found that in Plinian eruptions (MER $> 10^7$ kg/s) the latent heat released by condensation of vapor is relatively small in comparison with the thermal energy provided by the hot clasts and therefore moisture has no significant effect upon the eruption column dynamics. The largest influence of the phase change of water may occur for small or moderately sized eruptions where the energy released on condensation contributes significantly to the energy of the plume (Woods, 1993; Sparks et al., 1997; Woodhouse et al., 2013).

Due to gravity, particles tend to escape from the plume. This process was initially modeled by Woods & Bursik (1991), who assume that when a clast reaches a height at which the drag force equals its weight, the clast escapes from the plume. Moreover, due to the vortexes at the boundary of the plume, a fraction of the escaped particles may be re-entrained into the plume. The combined effect of fallout and re-entrainment was modeled by Bursik (2001) and is represented by eq. (1g) and (6). In this work, the effect of these processes (phase changes, entrainment of moisture, and particle fallout and re-entrainment) was investigated by turning off one process at a time and comparing with the reference runs. As observed in Figure 9 these effects are negligible for both strong and weak plumes. However, it should be stressed that the effect of moisture entrainment has been investigated only for the meteorological conditions of the reference tests. Previous works (eg. Woods, 1993; Bursik, 2001; Degruyter & Bonadonna, 2012) found that atmospheric humidity may have a significant effect on volcanic plumes. We expect that under other conditions (plumes in moist environment) the role of ambient moisture can become much more important.

5. Summary and discussion

We have performed a parametric and a sensitivity study to quantify how uncertainties in vent conditions and FPLUME plume model parameterizations affect the ESPs, in particular, the eruption column height. Uncertainties were explored within typical ranges for the two test cases (strong and weak) defined during the IAVCEI Commission on tephra hazard modeling inter-comparison study. The goal was to explore the leading order role of each parameter in order to assess which should be better constrained to better quantify ESPs for later use by TTDMs.

Results, summarized in Table 5, show that uncertainties in total MER at the vent $\hat{M}_o$ are the ones that most affect column height for both weak and strong plume cases. Conversely, uncertainties in plume height determination strongly impact on the source strength quantification (*e.g.* uncertainties of $\pm 20\%$ in h result on MER variations of roughly $\pm 50\%$). Uncertainties (variations) in wind entrainment coefficients and wind intensity are also of first order (consistent with results of Woodhouse et al., 2015), especially for the weak plume case. The combined effect of variations in α and β has a dramatic effect on the model results (see Fig. 7). In contrast, mixture exit velocity $\hat{u}_o$ and erupted water mass fraction $\hat{x}_{wo}$ have a second order effect for the considered range. Finally, the effect of mixture exit temperature $\hat{T}_o$ and particle size variations are almost negligible. Other physical phenomena such as water phase change, air humidity (moisture), and particle fallout and re-entrainment have been found to have little influence on model results for the test cases. However, it should be noted that atmospheric conditions have been not varied in our study. Other conditions different from those of the inter-comparison study (*e.g.* moist atmosphere) could result in notably different results.

Acknowledgments

This work was partially supported by the MED-SUV Project funded by the European Union (FP7 Grant Agreement n.308665). AC acknowledges a grant for visiting researchers of Earthquake Research Institute, Japan. The authors warmly thank the Guest Editors of JVGR Yujiro J. Suzuki (Univ. of Tokyo, Japan) for handling the paper and for the useful suggestions. Mattia de' Michieli Vitturi and Wim Degruyter are thanked for their constructive comments that have improved the manuscript.

Brown, R. J., Bonadonna, C., & Durant, A. J. (2012). A review of volcanic ash aggregation. *Phys. Chem. Earth*, *45-46*, 65–78. doi:10.1016/j.pce.2011.11.001.

Bursik, M. I. (2001). Effect of wind on the rise height of volcanic plumes. *Geophys. Res. Lett.*, *18*, 3621–3624.

Bursik, M. I., & Woods, A. W. (1991). Buoyant, superbuoyant and collapsing eruption columns. *J. Volcanol. Geotherm. Res.*, *45*, 347–350. doi:10.1016/0377-0273(91)90069-C.

Carazzo, G., Kaminski, E., & Tait, S. (2006). The route to self-similarity in turbulent jets and plumes. *J. Fluid Mech.*, *547*, 137–148. doi:10.1017/S002211200500683X.

Carazzo, G., Kaminski, E., & Tait, S. (2008a). On the dynamics of volcanic columns: A comparison of field data with new model of negatively buoyant jets. *J. Volcanol. Geotherm. Res.*, *178*, 94–103. doi:10.1016/j.jvolgeores.2008.01.002.

Carazzo, G., Kaminski, E., & Tait, S. (2008b). On the rise of turbulent plumes: Quantitative effects of variable entrainment for submarine hydrothermal vents, terrestrial and extra terrestrial explosive volcanism. *J. Geophys. Res.*, *113*. doi:10.1029/2007JB005458.

Costa, A., Folch, A., & Macedonio, G. (2010). A model for wet aggregation of ash particles in volcanic plumes and clouds: I. Theoretical formulation. *J. Geophys. Res.*, *115*. doi:10.1029/2009JB007175.

Costa, A., Folch, A., & Macedonio, G. (2013). Density-driven transport in the umbrella region of volcanic clouds: Implications for tephra dispersion models. *Geophys. Res. Lett.*, *40*, 1–5. doi:10.1002/grl.50942.

Costa, A., Macedonio, G., & Folch, A. (2006). A three-dimensional Eulerian model for transport and deposition of volcanic ashes. *Earth Planet. Sci. Lett.*, *241*, 634–647.

Costa, A., Suzuki, Y. J., Cerminara, M., Devenish, B. J., Esposti Ongaro, T., Herzog, M., Van Eaton, A. R., Denby, L. C., Bursik, M., de' Michieli Vitturi, M., Engwell, S., Neri, A., Barsotti, S., Folch, A., Macedonio, G., Girault, F., Carazzo, G., Tait, S., Kaminski, E., Mastin, L. G., Woodhouse, M. J., Phillips, J. C., Hogg, A. J., Degruyter, W., & Bonadonna, C. (2016). Results of the eruption column model inter-comparison study. *J. Volcanol. Geotherm. Res.*, . doi:10.1016/j.jvolgeores.2016.01.017.

Degruyter, W., & Bonadonna, C. (2012). Improving on mass flow rate estimates of volcanic eruptions. *Geophys. Res. Lett.*, *39*, L16308. doi:10.1029/2012GL052566.

Degruyter, W., & Bonadonna, C. (2013). Impact of wind on the condition for column collapse of volcanic plumes. *Earth Planet. Sci. Lett.*, *377-378*, 218–226. doi:10.1016/j.epsl.2013.06.041.

Dellino, P., Dioguardi, F., Mele, D., D'Addabbo, M., Zimanowski, B., Büttner, R., Doronzo, D. M., Sonder, I., Sulpizio, R., Dürig, T., & La Volpe, L. (2014). Volcanic jets, plumes, and collapsing fountains: evidence from large-scale experiments, with particular emphasis on the entrainment rate. *Bull. Volcanol.*, *76*, 834. doi:10.1007/s00445-014-0834-6.

Devenish, B. J. (2013). Using simple plume models to refine the source mass flux of volcanic eruptions according to atmospheric conditions. *J. Volcanol. Geotherm. Res.*, *256*, 118–127. doi:10.1016/j.jvolgeores.2013.02.015.

Ernst, G. J., Sparks, R. S. J., Carey, S. N., & Bursik, M. I. (1996). Sedimentation from turbulent jets and plumes. *J. Geophys. Res.*, *101*, 5575–5589. doi:10.1029/95JB01900.

Folch, A. (2012). A review of tephra transport and dispersal models: Evolution, current status, and future perspectives. *J. Volcanol. Geotherm. Res.*, *235-236*, 96–115. doi:10.1016/j.jvolgeores.2012.05.020.

Folch, A., Costa, A., & Basart, S. (2012). Validation of the FALL3D ash dispersion model using observations of the 2010 Eyjafjallajokull volcanic ash cloud. *Atmos. Environ.*, *48*, 165–183. doi:10.1016/j.atmosenv.2011.06.072.

Folch, A., Costa, A., & Macedonio, G. (2009). FALL3D: A computational model for transport and deposition of volcanic ash. *Comput. Geosci.*, *35*, 1334–1342. doi:10.1016/j.cageo.2008.08.008.

Folch, A., Costa, A., & Macedonio, G. (2016). FPLUME-1.0: An integral volcanic plume model accounting for ash aggregation. *Geosci. Model Dev.*, *9*, 431–450. doi:10.5194/gmd-9-431-2016.

Ganser, G. H. (1993). A rational approach to drag prediction of spherical and nonspherical particles. *Powder Technol.*, *77*, 143–152. doi:10.1016/0032-5910(93)80051-B.

Girault, F., Carazzo, G., Ferrucci, F., & Kaminski, E. (2014). The effect of total grain-size distribution on the dynamics of turbulent volcanic plumes. *Earth Planet. Sci. Lett.*, *394*, 124–134. doi:10.1016/j.epsl.2014.03.021.

Girault, F., Carazzo, G., Tait, S., & Kaminski, E. (2016). Combined effects of total grain-size distribution and crosswind on the rise of eruptive volcanic columns. *J. Volcanol. Geotherm. Res.*, . doi:10.1016/j.jvolgeores.2015.11.007.

Hashimoto, A., Shimbori, T., & Fukui, K. (2012). Tephra fall simulation for the eruptions at Mt. Shinmoe-dake during 26-27 January 2011 with JMANHM. *SOLA*, *8*, 37–40. doi:10.2151/sola.2012-010.

Hewett, T. A., Fay, J. A., & Hoult, D. P. (1971). Laboratory experiments of smokestack plumes in a stable atmosphere. *Atmos. Environ.*, *5*, 767–789. doi:10.1016/0004-6981(71)90028-X.

Kaminski, E., & Jaupart, C. (2001). Marginal stability of atmospheric eruption columns and pyroclastic flow generation. *J. Geophys. Res.*, *106*, 21,785–21,798. doi:10.1029/2001JB000215.

Mastin, L. G. (2014). Testing the accuracy of a 1-D volcanic plume model in estimating mass eruption rate. *J. Geophys. Res. Atmos.*, *119*, 2474–2495. doi:10.1002/2013JD020604.

de' Michieli Vitturi, M., Neri, A., & Barsotti, S. (2015). PLUME-MoM 1.0: A new integral model of volcanic plumes masede on the method of moments. *Geosci. Model Dev.*, *8*, 2447–2463. doi:10.5194/gmd-8-2447-2015.

Morton, B. R., Taylor, G., & Turner, J. S. (1956). Turbulent gravitational convection from mantained and instantaneous sources. *Proc. Roy. Soc. London, Ser. A*, *234*, 1–23.

Pouget, S., Bursik, M., Singla, P., & Singh, T. (2016). Sensitivity analysis of a one-dimensional model of a volcanic plume with particle fallout and collapse behavior. *J. Volcanol. Geotherm. Res.*, . doi:10.1016/j.jvolgeores.2016.02.018.

Schwaiger, H. F., Denlinger, R. P., & Mastin, L. G. (2012). Ash3d: A finite-volume, conservative numerical model for ash transport and tephra deposition. *J. Geophys. Res.*, *117*, B04204. doi:10.1029/2011JB008968.

Settle, M. (1978). Volcanic eruption clouds and the thermal power output of explosive eruptions. *J. Volcanol. Geotherm. Res.*, *3*, 309–324.

Sparks, R. S. J. (1986). The dimensions and dynamics of volcanic eruption columns. *Bull. Volcanol.*, *48*, 3–15. doi:10.1007/BF01073509.

Sparks, R. S. J., Bursik, M. I., Carey, S. N., Gilbert, J. S., Glaze, L. S., Sigurdsson, H., & Woods, A. W. (1997). *Volcanic Plumes*. Chichester, U.K.: John Wiley & Sons Ltd.

Sparks, R. S. J., & Wilson, L. (1976). A model for the formation of ignimbrite by gravitational column collapse. *J. Geol. Soc. London*, *132*, 441–451. doi:10.1144/gsjgs.132.4.0441.

Suzuki, Y. J., & Koyaguchi, T. (2015). Effects of wind on entrainment efficiency in volcanic plumes. *J. Geophys. Res.*, *110*, 6122–6140. doi:10.1002/2015JB012208.

Tate, P. M. (2002). *The rise and dilution of buoyant jets and their behaviour in an internal wave field*. Phd thesis University of New South Wales, School of Mathematics. URL: `http://trove.nla.gov.au/version/19798635` last access: 16 September 2015.

Tate, P. M., & Middleton, J. H. (2000). Unification of non-dimensional solutions to asymptotic equations for plumes of different shape. *Boundary-Layer Meteorol.*, *94*, 225–251.

Valentine, G. A., & Wohletz, K. H. (1989). Numerical models of Plinian eruption columns and pyroclastic flows. *J. Geophys. Res.*, *94*, 1867–1887. doi:10.1029/JB094iB02p01867.

Wilson, L. (1976). Explosive volcanic eruptions III. Plinian eruption columns. *Geophys. J. R. Astron. Soc.*, *45*, 543–556.

Wilson, L., Sparks, R. S. J., Huang, T. C., & Watkins, N. D. (1978). The control of volcanic column heights by eruption energetics and dynamics. *J. Geophys. Res.*, *83*, 1829–1836. doi:10.1029/JB083iB04p01829.

Wilson, L., Sparks, R. S. J., & Walker, G. P. L. (1980). Explosive volcanic eruptions IV. The control of magma properties and conduit geometry on eruption column behavior. *Geophys. J. R. Astron. Soc.*, *63*, 117–148.

Woodhouse, M. J., Hogg, A. J., Phillips, J. C., & Rougier, J. C. (2015). Uncertainty analysis of a model of wind-blown volcanic plumes. *Bull. Volcanol.*, *77*, 83. doi:10.1007/s00445-015-0959-2.

Woodhouse, M. J., Hogg, A. J., Phillips, J. C., & Sparks, R. S. J. (2013). Interaction between volcanic plumes and wind during the 2010 Eyjafjallajökull eruption, Iceland. *J. Geophys. Res. Solid Earth*, *118*, 92–109. doi:10.1029/2012JB009592.

Woods, A. W. (1988). The fluid dynamics and thermodynamics of eruption columns. *Bull. Volcanol.*, *50*, 169–193.

Woods, A. W. (1993). Moist convection and the injection of volcanic ash into the atmosphere. *J. Geophys. Res.*, *98*, 17,627–17,636.

Woods, A. W., & Bursik, M. I. (1991). Particle fallout, thermal disequilibrium and volcanic plumes. *Bull. Volcanol.*, *53*, 559–570. doi:10.1007/BF00298156.

Table 1: List of latin symbols. Quantities with a hat denote bulk (top-hat averaged) quantities. Throughout the text, the subindex o (*e.g.* $\hat{M}_o$, $\hat{u}_o$, etc.) indicates values of quantities at the vent ($s = 0$).

Symbol	Definition	Units
$A_i^+ (A_i^-)$	Aggregation source (sink) terms	$\mathrm{kg\,s^{-1}m^{-1}}$
c_a	Specific heat capacity of air at constant pressure	$\mathrm{J\,kg^{-1}\,K^{-1}}$
c_l	Specific heat capacity of liquid water	$\mathrm{J\,kg^{-1}\,K^{-1}}$
c_p	Specific heat capacity of particles (pyroclasts)	$\mathrm{J\,kg^{-1}\,K^{-1}}$
c_s	Specific heat capacity of solid water (ice)	$\mathrm{J\,kg^{-1}\,K^{-1}}$
c_v	Specific heat capacity of water vapor	$\mathrm{J\,kg^{-1}\,K^{-1}}$
c_w	Specific heat capacity of water (generic)	$\mathrm{J\,kg^{-1}\,K^{-1}}$
$\hat{E}$	Energy flow rate	$\mathrm{J\,s^{-1}}$
f_i	Mass fraction of particle class i	—
g	Gravitational acceleration	$\mathrm{m\,s^{-2}}$
h	Column height	m
h_l	Enthalpy per unit mass of liquid water	$\mathrm{J\,kg^{-1}}$
h_s	Enthalpy per unit mass of ice	$\mathrm{J\,kg^{-1}}$
h_v	Enthalpy per unit mass of vapour	$\mathrm{J\,kg^{-1}}$
h_{l0}	Enthalpy per unit mass of liquid water at $T = T_0$	$\mathrm{J\,kg^{-1}}$
h_{s0}	Enthalpy per unit mass of ice at $T = T_0$	$\mathrm{J\,kg^{-1}}$
h_{v0}	Enthalpy per unit mass of vapour at $T = T_0$	$\mathrm{J\,kg^{-1}}$
$\hat{H}$	Enthalpy flow rate	$\mathrm{J\,s^{-1}}$
m_a	Molar weight of air	kg/mole
m_v	Molar weight of water	kg/mole
$\hat{M}$	Total mass flow rate	$\mathrm{kg\,s^{-1}}$
$\hat{M}_a$	Mass flow rate of dry air	$\mathrm{kg\,s^{-1}}$
$\hat{M}_i$	Mass flow rate of particles of class i	$\mathrm{kg\,s^{-1}}$
$\hat{M}_w$	Mass flow rate of volatiles (water in any phase)	$\mathrm{kg\,s^{-1}}$
n_a	Molar fraction of air in the gas phase	—
n_v	Molar fraction of vapour in the gas phase	—
$\hat{P}$	Axial (stream-wise) momentum flow rate	$\mathrm{kg\,m\,s^{-2}}$
P	Pressure	Pa
P_a	Partial pressure of air	Pa
P_v	Partial pressure of water vapor	Pa
s	Distance along the plume axis	m
$\hat{T}$	Mixture temperature	K
T_a	Ambient air temperature	K
T_0	Reference temperature (273.15 K)	K
$\hat{u}$	Mixture velocity along the plume axis	$\mathrm{m\,s^{-1}}$
u_a	Horizontal wind (air) velocity	$\mathrm{m\,s^{-1}}$
u_e	Air entrainment velocity (by turbulent eddies)	$\mathrm{m}\,s^{-1}$
w_a	Mass fraction of water in the entrained ambient air	-
x	Horizontal coordinate	m
x_l	Mass fraction of liquid water	—
x_s	Mass fraction of solid water (ice)	—
x_v	Mass fraction of water vapor	—
x_p	Mass fraction of particles (pyroclasts)	—
x_w	Mass fraction of volatiles (water)	—
y	Horizontal coordinate	m
z	Vertical coordinate	m

Table 2: List of greek symbols.

Symbol	Definition	Units
α	stream-wise (shear) air entrainment coefficient	-
β	cross-flow (vortex) air entrainment coefficient	-
$\hat{\rho}$	Mixture density	$\mathrm{kg\,m^{-3}}$
ρ_a	Ambient air density	$\mathrm{kg\,m^{-3}}$
Φ_a	Horizontal wind direction (azimuth)	rad
Ψ	Particle sphericity	-
χ	Constant giving the probability of fallout	-

Table 3: Reference values of the parameters for the strong and weak plume cases (Costa et al., 2016).

Parameter	**Symbol**	**Units**	**Strong**	**Weak**
Mass flow rate	M	kg/s	1.5×10^9	1.5×10^6
Vent height (a.s.l)	h_v	m	1500	1500
Velocity at the vent	u_0	m/s	275	135
Temperature at the vent	T_0	K	1053	1273
Water mass fraction at the vent	w_0	—	5%	3%

Table 4: Total particle grain size distribution at the vent for strong and weak plumes discretized in n=14 classes. The Φ units are defined so that the particle diameter (in mm) is $d = 2^{-\Phi}$. The sphericity parameter Ψ is assumed equal to 0.9. The mean particle densities are 2646.3 and 2414.4 $\mathrm{kg/m^3}$, respectively for the strong and the weak plumes.

Diameter		**Strong Plumes**		**Weak Plumes**	
		Density	**wt.%**	**Density**	**wt.%**
(Φ)	(mm or μm)	($\mathrm{kg/m^3}$)	(—)	($\mathrm{kg/m^3}$)	(—)
-6	64	—	—	1700.0	0.01
-5	32	2200.0	0.01	1792.3	0.11
-4	16	2253.8	0.10	1884.6	0.59
-3	8	2307.7	0.59	1976.9	2.24
-2	4	2361.5	2.23	2069.2	5.77
-1	2	2415.4	5.76	2161.5	10.26
0	1	2469.2	10.16	2253.8	12.86
1	500	2523.1	12.37	2346.2	12.39
2	250	2576.9	10.74	2438.5	11.52
3	125	2630.8	7.99	2530.8	12.39
4	62.5	2684.6	7.99	2623.1	12.86
5	31.25	2738.5	10.74	2715.4	10.26
6	15.62	2792.3	12.37	2807.7	5.77
7	7.8	2846.2	10.16	2900.0	2.96
8	3.9	2900.0	8.71	—	—

Table 5: Summary of results. Effect of input uncertainties on column height expressed as h/h^{ref} (*i.e.* values close to 1 imply little effect.)

Parameter	Case	wind	Increase range	h/h^{ref}	Decrease range	h/h^{ref}
$\hat{M}_o$	strong	no	$\hat{M}_o \times 3.3^{(*)}$	1.35	$\hat{M}_o \times 1/5$	0.72
		yes	$\hat{M}_o \times 5$	1.48	$\hat{M}_o \times 1/5$	0.72
	weak	no	$\hat{M}_o \times 5$	1.39	$\hat{M}_o \times 1/5$	0.62
		yes	$\hat{M}_o \times 5$	1.78	$\hat{M}_o \times 1/5$	0.64
$\hat{u}_o$	strong	no	$\hat{u}_o + 30\%$	0.93	$\hat{u}_o - 17\%^{(*)}$	1.05
		yes	$\hat{u}_o + 30\%$	0.93	$\hat{u}_o - 30\%$	1.06
	weak	no	$\hat{u}_o + 30\%$	0.99	$\hat{u}_o - 30\%$	1.02
		yes	$\hat{u}_o + 30\%$	0.99	$\hat{u}_o - 30\%$	1.03
$\hat{T}_o$	strong	no	$\hat{T}_o + 100\,\mathrm{K}$	1.02	$\hat{T}_o - 100\,\mathrm{K}$	0.97
		yes	$\hat{T}_o + 100\,\mathrm{K}$	1.02	$\hat{T}_o - 100\,\mathrm{K}$	0.97
	weak	no	$\hat{T}_o + 100\,\mathrm{K}$	negligible	$\hat{T}_o - 100\,\mathrm{K}$	negligible
		yes	$\hat{T}_o + 100\,\mathrm{K}$	negligible	$\hat{T}_o - 100\,\mathrm{K}$	negligible
x_{wo}	strong	no	$x_{wo} + 2$ wt%	1.04	$x_{wo} - 2$ wt%	0.97
		yes	$x_{wo} + 2$ wt%	1.04	$x_{wo} - 2$ wt%	0.95
	weak	no	$x_{wo} + 2$ wt%	1.04	$x_{wo} - 2$ wt%	0.96
		yes	$x_{wo} + 2$ wt%	1.03	$x_{wo} - 2$ wt%	0.97
particle size	strong	no	$\Phi_o + 4\Phi$	negligible	$\Phi_o - 4\Phi$	0.96
(1 class at		yes	$\Phi_o + 4\Phi$	negligible	$\Phi_o - 4\Phi$	negligible
$\Phi_o = 2$)	weak	no	$\Phi_o + 4\Phi$	negligible	$\Phi_o - 4\Phi$	0.85
		yes	$\Phi_o + 4\Phi$	negligible	$\Phi_o - 4\Phi$	negligible
Wind entrainment	strong	no	$\alpha_o + 0.05$	0.90	$\alpha_o - 0.05$	1.16
coefficients		yes	$\alpha_o + 0.05, \beta_o + 1.0$	0.87	$\alpha_o - 0.05, \beta_o$	1.16
$\alpha_o = 0.1$	weak	no	$\alpha_o + 0.05$	0.88	$\alpha_o - 0.05$	1.27
$\beta_o = 0.0$		yes	$\alpha_o + 0.05, \beta_o + 1.0$	0.38	$\alpha_o - 0.05, \beta_o$	1.27
Wind intensity	strong	yes	$f_w \in (1,2)$	0.95	$f_w \in (0,1)$	1.08
f_w	weak	yes	$f_w \in (1,2)$	0.83	$f_w \in (0,1)$	1.82

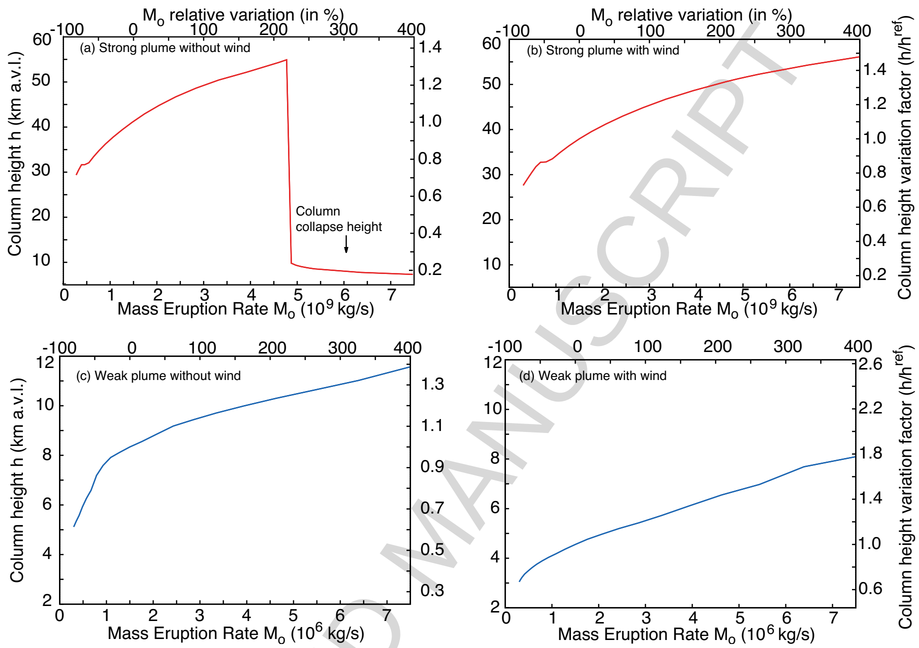

Figure 1: Variation of the column height as function of the mass eruption rate (MER) for the strong (top) and weak (bottom) plumes without (left) and with (right) wind. The top and right axes indicate, respectively, the relative MER variation with respect to the reference value (1.5×10^9 and 1.5×10^6 kg/s for strong and weak plumes respectively) and its effect on the column height. Note that, in absence of wind, the column collapses for MER larger than about 4.9×10^9 kg/s. For the strong plume case (red lines), the small bumps in the left part of the plots are due to the effect of water phase change.

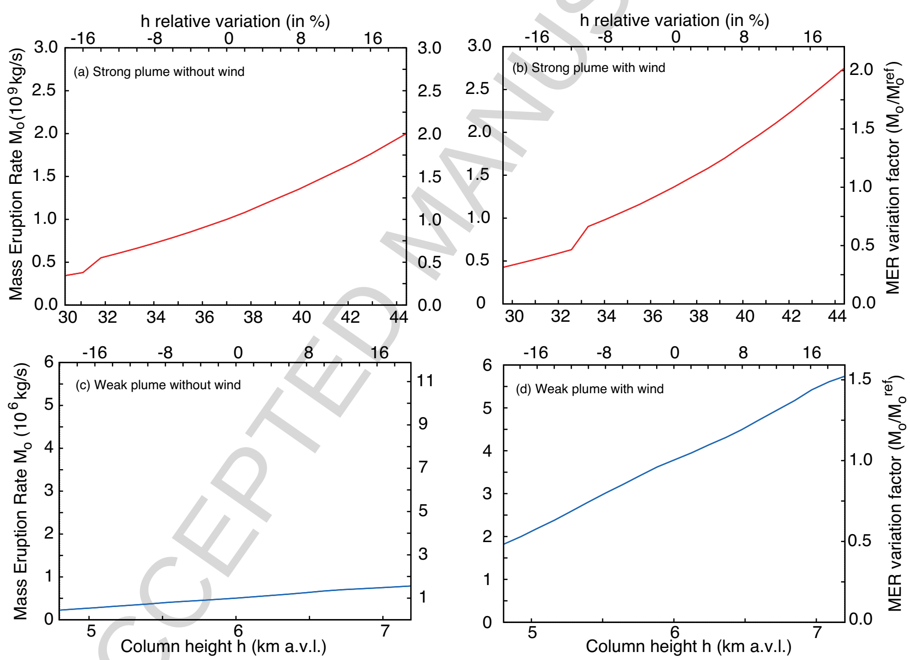

Figure 2: Variation of the mass eruption rate (MER) with column height for the strong (top) and weak (bottom) plumes without (left) and with (right) wind. The top and right axes indicate, respectively, the column height variation with respect to the reference values (37 and 6 km for strong and weak respectively) and its effect on the MER. For the strong plume case (red lines), the small bumps in the left part of the plots are due to the effect of water phase change. Note that plots agree with Figure 1 in the ranges shown.

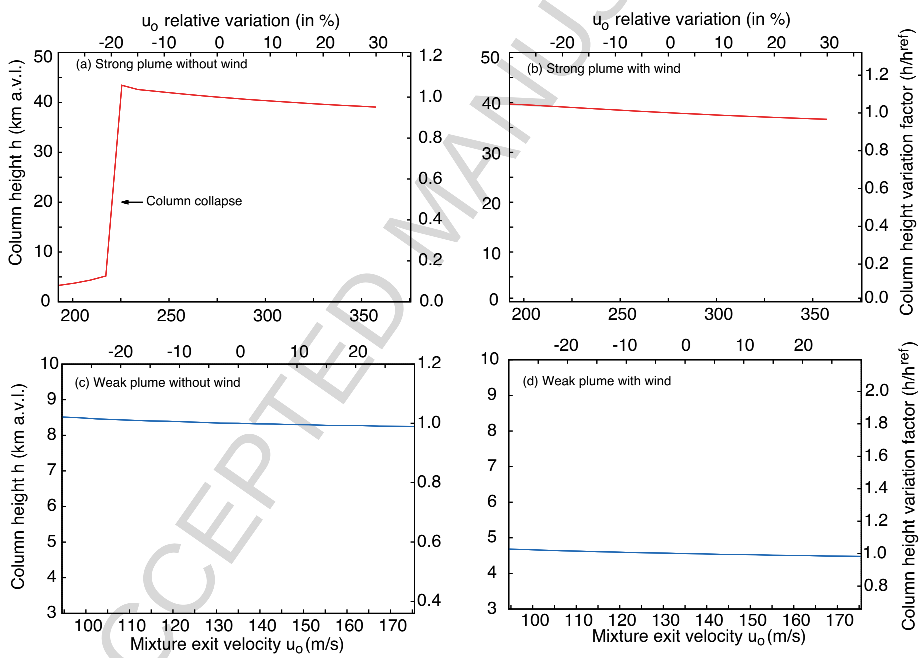

Figure 3: Variation of column height with plume velocity at the vent for the strong (top) and weak (bottom) plumes without (left) and with (right) wind. The top and right axes indicate, respectively, the exit velocity variation with respect to the reference values (275 and 135 m/s for strong and weak respectively) and its effect on the column height. Note that, in absence of wind, the column collapses if velocities at the vent are smaller than about 220 m/s.

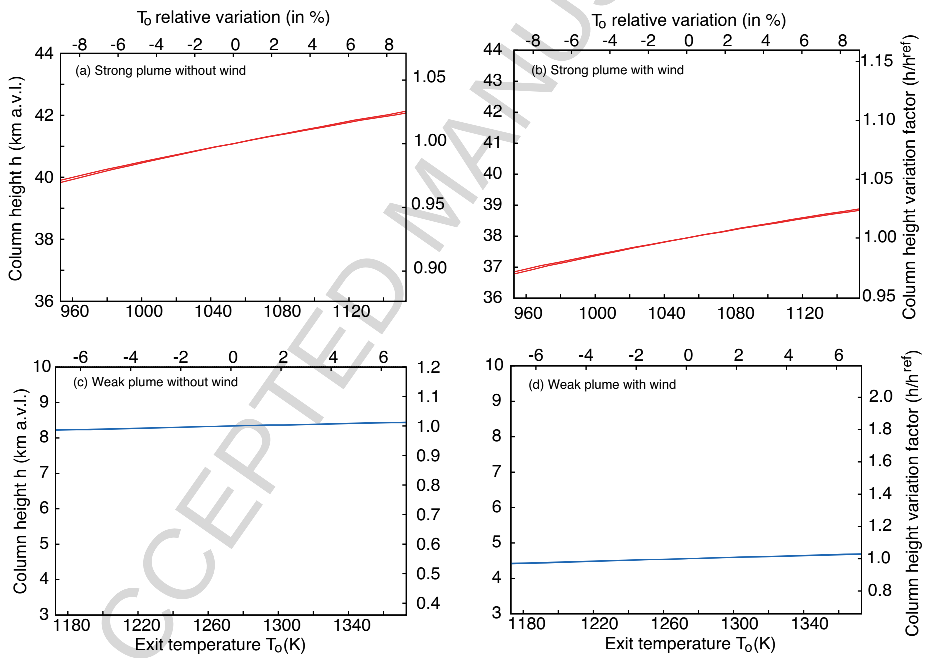

Figure 4: Variation of column height with temperature at the vent for the strong (top) and weak (bottom) plumes without (left) and with (right) wind. The top and right axes indicate, respectively, the temperature variation with respect to the reference values (1053 and 1273 K for strong and weak respectively) and its effect on the column height.

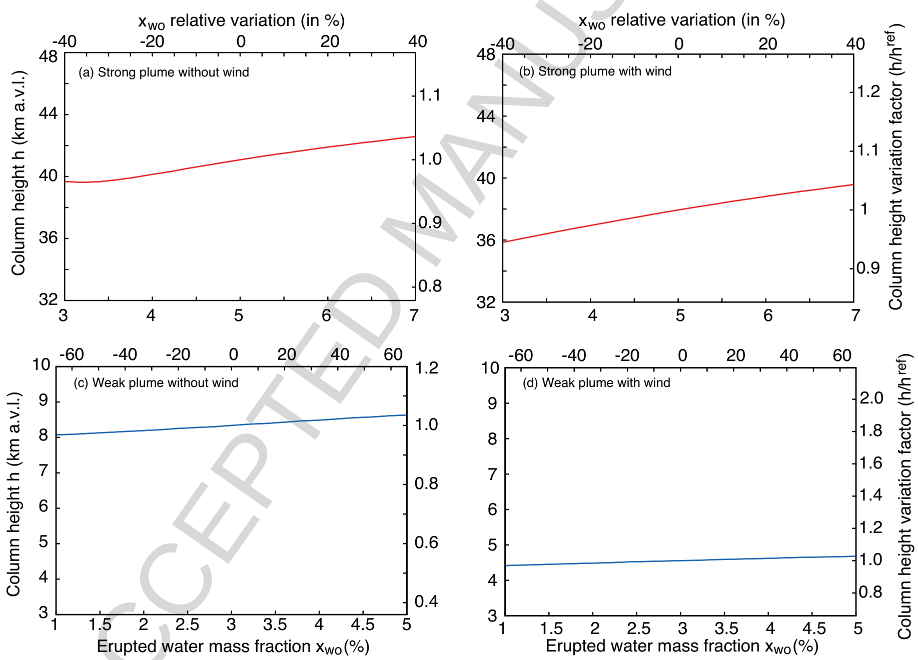

Figure 5: Variation of column height with initial water content for the strong (top) and weak (bottom) plumes without (left) and with (right) wind. The top and right axes indicate, respectively, the variation of water content with respect to the reference values (5 and 3% for strong and weak respectively) and its effect on the column height. Mass eruption rate, exit velocity and temperature are kept fixed, whereas vent radius is allowed to vary.

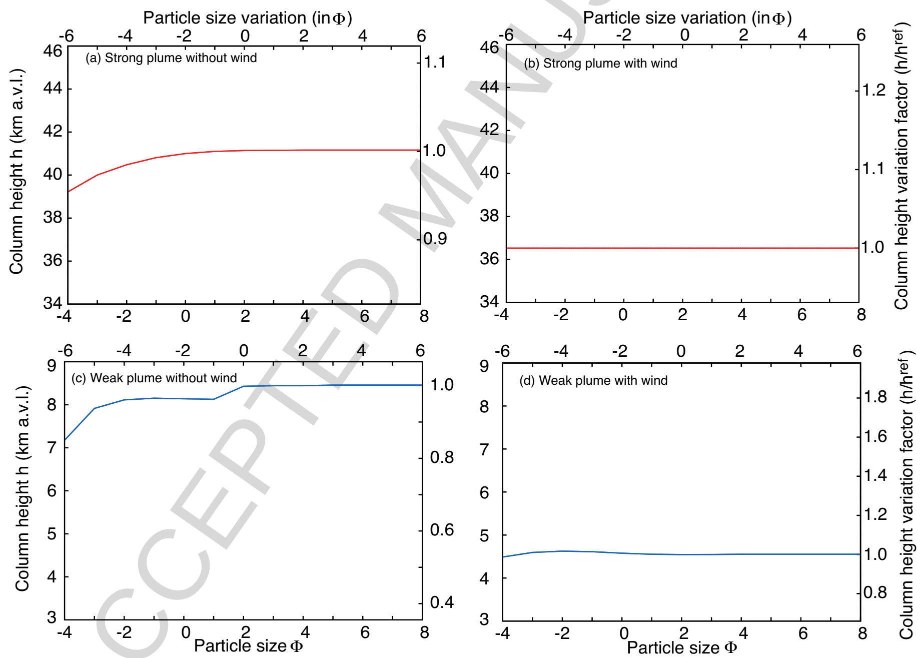

Figure 6: Variation of column height with particle grain size for the strong (top) and weak (bottom) plumes without (left) and with (right) wind. Note that one single class is assumed in these particular runs. The top and right axes indicate, respectively, the variation of class size with respect to a reference value ($\Phi = 2$) and its effect on the column height.

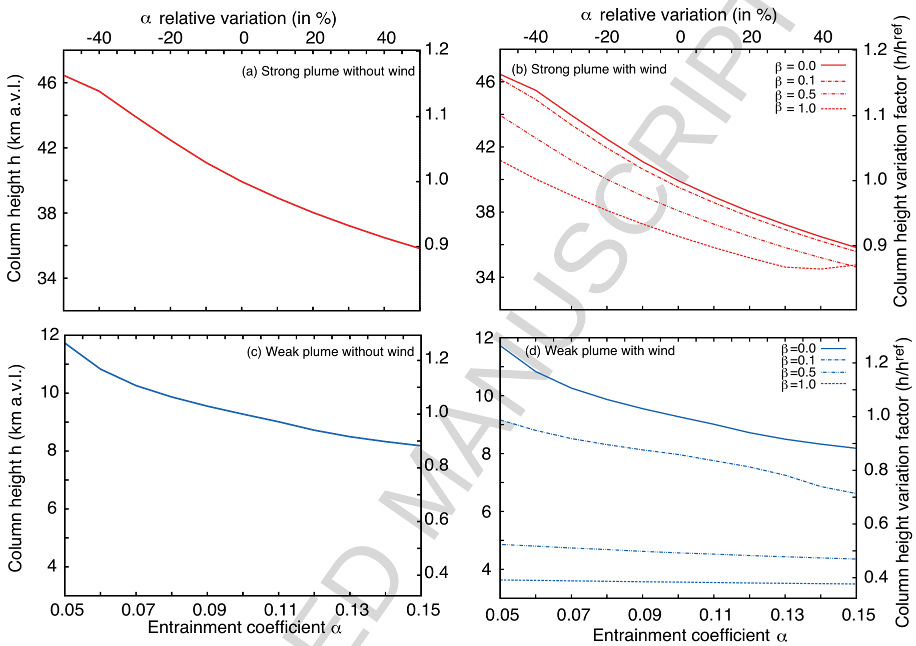

Figure 7: Variation of column height with entrainment coefficient α for the strong (top) and weak (bottom) plumes without (left) and with (right) wind. The top and right axes indicate, respectively, the variation of α with respect to the reference value ($\alpha = 0.1$) and its effect on the column height. In case of wind, results are given for different β values of 0, 0.1, 0.5 and 1.

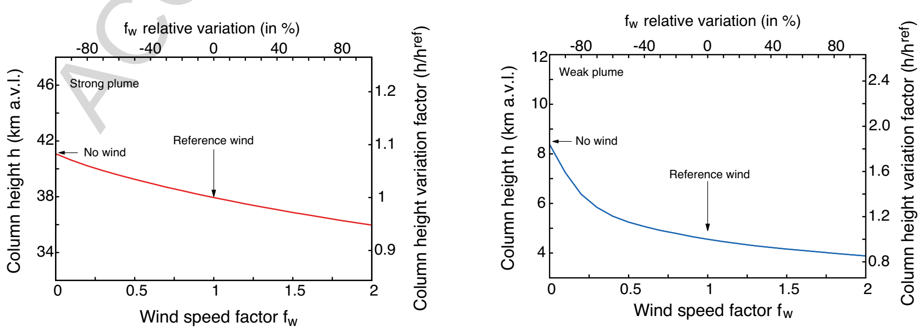

Figure 8: Variation of the column height depending on wind intensity (wind speed factor f_w) for strong (left) and weak (right) plumes. A value of $f_w = 1.0$ corresponds to the reference wind used in this work whereas a value of $f_w = 0.0$ corresponds to plumes in absence of wind. The top and right axes indicate, respectively, the variation of wind speed factor with respect the reference values and its effect on the column height.

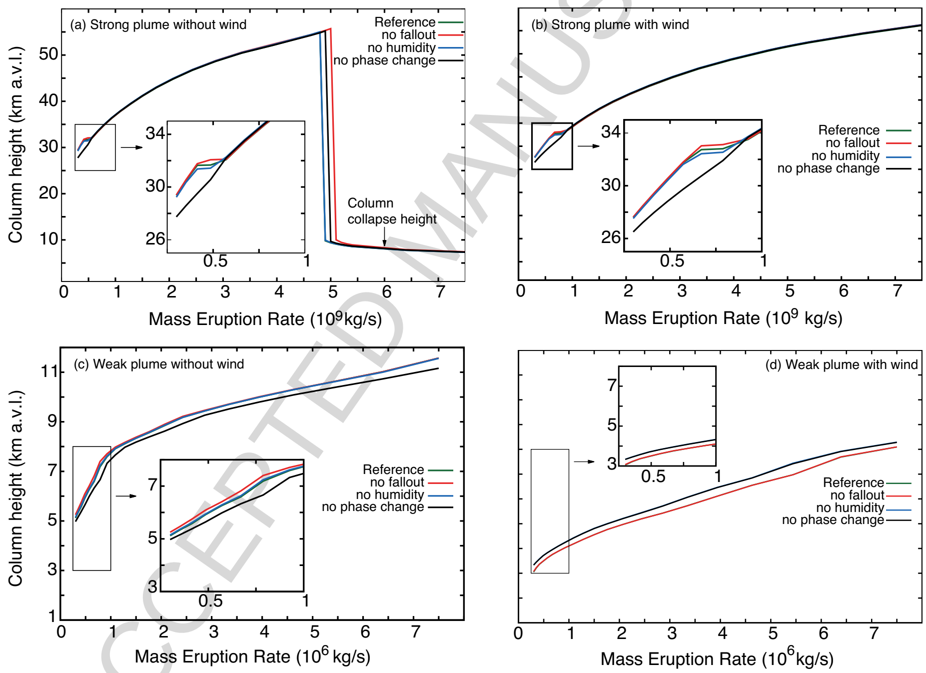

Figure 9: Variation of the column height as function of the mass eruption rate (MER) for the strong (top) and weak (bottom) plumes without (left) and with (right) wind. The reference simulations (green lines) are compared with those obtained by neglecting particle fallout (red lines), atmospheric humidity (blue lines) and the water phase change (black lines). Note that, in absence of wind, the column collapses for MER larger than about 5×10^9 kg/s. The small bumps in the left part of the plots (zoomed areas) are due to the effect of water phase change.

Highlights

- We perform a sensitivity study on input parameters of a volcanic plume model
- Effects of input parameter variation on plume model results were estimated
- Effects on entrainment parameter variation and wind intensity was estimated
- Typical uncertainty on mass flow rate and plume height estimation was assessed